J. Mech. Phys. Solids Vol. 41, No. 8, pp. 1265–1284, 1993.
Printed in Great Britain.

0022–5096/93 $6.00 + 0.00

COMPRESSIVE FATIGUE OF FIBRE COMPOSITES

W. S. SLAUGHTER and N. A. FLECK
Cambridge University Engineering Department, Cambridge CB2 1PZ, U.K.

(*Received* 16 *November* 1992; *in revised form* 26 *April* 1993)

ABSTRACT

FIBRE COMPOSITES may fail under compression–compression fatigue loading by microbuckling. A detailed analysis of fatigue failure is presented, based on two alternative constitutive laws: the Mroz plasticity law and the Armstrong and Frederick ratchetting law. Failure is anticipated to occur by a low cycle fatigue process in materials which obey the Mroz law, and by plastic instability in materials which exhibit pronounced cyclic ratchetting. Predictions of the two theories are compared with available experimental data.

INTRODUCTION

A DESIGN limiting factor in the utilization of aligned fibre composites is their relatively low compressive strength. This can be less than 60% of one composite's tensile strength. The dominant mechanism in the monotonic compressive failure of aligned fibre composites is microbuckling (ARGON, 1972; BUDIANSKY and FLECK, 1993). Microbuckling is also an important mechanism in the compressive fatigue failure of polymer matrix and metal matrix-aligned fibre composites (HUANG and WANG, 1989). In this paper, a theoretical model of compressive fatigue microbuckling is proposed.

The compressive fatigue analysis of this paper is based on a model developed by BUDIANSKY and FLECK (1993) to analyse monotonic compressive failure of fibre composites. This monotonic microbuckling model includes the effects of matrix yielding and initial imperfections in the form of fibre misalignment. The analysis follows the non-linear plastic collapse response of an imperfect structure. It is not a bifurcation analysis. Analyses which treat microbuckling as a linear elastic buckling phenomenon (e.g. ROSEN, 1965) significantly overestimate the critical stress necessary for microbuckling. In the Budiansky and Fleck model the assumption is made that a band of misaligned fibres exists and that the composite exhibits a predilection to microbuckle uniformly within this band. This band of initial misalignment is not, in general, normal to the fibre direction. The fibres are assumed to be inextensible and have no bending stiffness. Recent studies have shown that these are acceptable approximations (FLECK *et al.*, 1993). The aforementioned assumptions lead to kinematic constraints and equations of equilibrium which will be used in the fatigue microbuckling analysis of this paper.

Two different cyclic plasticity theories are used to describe the constitutive behav-

iour of the composite. The first of these is the Mroz multiyield surface generalization of Prager's kinematic hardening rule (MROZ, 1967; CHABOCHE, 1986) which is fitted to the Ramberg–Osgood strain hardening relation. It will be shown that proportional loading is maintained within the kink band, allowing the Mroz flow theory relations to be integrated in closed form. Fatigue failure is predicted using a Coffin–Manson type low-cycle fatigue law (HERTZBERG, 1976). Plastic strain accumulation, hereafter referred to as ratchetting, does not occur in the Mroz theory. To examine the effects of ratchetting, a second cyclic plasticity theory is adopted. This is the non-linear kinematic hardening rule first proposed by ARMSTRONG and FREDERICK (1966), in which the kinematic hardening variables are governed by a differential equation (CHABOCHE, 1986). Progressive deformation of the kink band by ratchetting culminates in a plastic instability.

MICROBUCKLING UNDER MONOTONIC LOADING

Microbuckling is a phenomenon in which localized deformation occurs within a kink band. This kink band is not, in general, normal to the fibre direction and is of the order of 10 fibre diameters in width. In this paper, the kink band will be modelled as shown in Fig. 1. The kink band forms an angle β with the direction normal to the fibres and has a width w. It is assumed that the fibres are inextensible and that the kink band deformation is given by the fibre rotation ϕ. It is also assumed that the initial composite fibre misalignment can be approximated by an initial kink band fibre

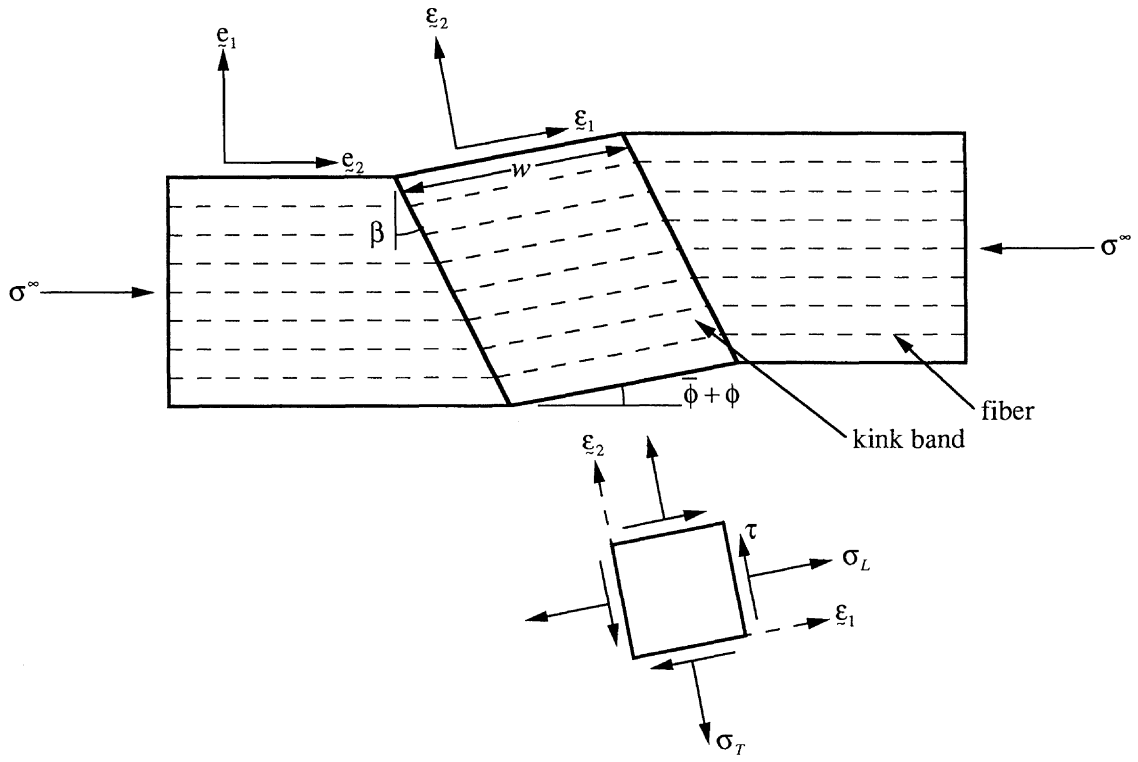

FIG. 1. Kink band geometry and notation.

rotation $\bar{\phi}$. Two coordinate systems are defined, $(\mathbf{e}_1, \mathbf{e}_2)$ and $(\boldsymbol{\varepsilon}_1, \boldsymbol{\varepsilon}_2)$, aligned with the fibre direction outside and inside the kink band, respectively. The only remote loading considered here is pure axial compression, $\boldsymbol{\sigma}^\infty = -\sigma^\infty \mathbf{e}_1\mathbf{e}_1$.

Within the kink band the stress is given by $\boldsymbol{\sigma} = \sigma_L \boldsymbol{\varepsilon}_1\boldsymbol{\varepsilon}_1 + \sigma_T \boldsymbol{\varepsilon}_2\boldsymbol{\varepsilon}_2 + \tau(\boldsymbol{\varepsilon}_1\boldsymbol{\varepsilon}_2 + \boldsymbol{\varepsilon}_2\boldsymbol{\varepsilon}_1)$ and the strain is given by $\mathbf{e} = e_T \boldsymbol{\varepsilon}_2\boldsymbol{\varepsilon}_2 + \frac{1}{2}\gamma(\boldsymbol{\varepsilon}_1\boldsymbol{\varepsilon}_2 + \boldsymbol{\varepsilon}_2\boldsymbol{\varepsilon}_1)$. Expressions for kinematic conditions and continuity of tractions across the kink band interface have been derived by BUDIANSKY and FLECK (1993). In the $\boldsymbol{\varepsilon}_2$ direction perpendicular to the kink band fibres, continuity of tractions requires

$$\sigma^\infty \cos\beta \sin(\bar{\phi}+\phi) = \tau \cos(\beta-\bar{\phi}-\phi) + \sigma_T \sin(\beta-\bar{\phi}-\phi). \tag{1}$$

Anticipating that, in the analyses to follow, small values of ϕ and $\bar{\phi}$ will be sufficient to describe the fatigue microbuckling phenomenon, (1) can be reduced to the approximate equilibrium statement

$$\sigma^\infty \approx \frac{\tau + \sigma_T \tan\beta}{\bar{\phi}+\phi}. \tag{2}$$

Also for small ϕ and $\bar{\phi}$, the appropriate kinematic equations relating strains within the kink band to ϕ are (BUDIANSKY and FLECK, 1993)

$$\left.\begin{aligned} \gamma &\approx \phi \\ e_T &\approx \phi \tan\beta \end{aligned}\right\}. \tag{3}$$

In the absence of shear straining outside the kink band, the kink band angle β remains constant. Note that (3) imply proportional *straining*; proportional *loading* is established below. Following BUDIANSKY and FLECK (1993), a solution scheme for calculating the critical microbuckling stress σ_c^∞ is now outlined. The scheme will then be extended for the case of fatigue loading.

Assume that the composite material is characterized by the quadratic yield condition

$$\left(\frac{\tau}{\tau_y}\right)^2 + \left(\frac{\sigma_T}{\sigma_{Ty}}\right)^2 = 1 \tag{4}$$

where τ_y and σ_{Ty} are the plain strain yield stresses in pure shear and pure transverse tension, respectively. The parameter $R \equiv \sigma_{Ty}/\tau_y$ defines the eccentricity of the yield ellipse. An effective stress τ_e, defined by

$$\tau_e \equiv \sqrt{\tau^2 + (\sigma_T/R)^2}, \tag{5}$$

is used as a plastic potential for the plastic strain rates, $\dot{\gamma}^p$ and $\dot{e}_T^p$. For an increment of plastic loading, the associated flow theory relations for plastic strain rates, based on τ_e as a plastic potential, can be written as

$$\left.\begin{aligned} \dot{\gamma}^p &= F(\tau_e)\frac{\partial \tau_e}{\partial t}\dot{\tau}_e \\ \dot{e}_T^p &= F(\tau_e)\frac{\partial \tau_e}{\partial \sigma_T}\dot{\tau}_e \end{aligned}\right\} \tag{6}$$

where $F(\tau_e)$ is a measure of the rate of strain hardening. A work equivalent effective plastic strain rate, $\dot{\gamma}_e^p$, is defined by

$$\tau\dot{\gamma}^p + \sigma_T \dot{e}_T^p = \tau_e \dot{\gamma}_e^p \tag{7}$$

and it follows that

$$\dot{\gamma}_e^p = F(\tau_e)\dot{\tau}_e = \sqrt{(\dot{\gamma}^p)^2 + R^2(\dot{e}_T^p)^2}. \tag{8}$$

From (8), $F(\tau_e)$ is interpreted as the inverse of the pure shear tangent modulus minus the inverse of the elastic shear modulus. Substituting (8) into (6) and anticipating that proportional loading will be established leads to

$$\left.\begin{aligned} \gamma^p &= \left(\frac{\gamma_e^p}{\tau_e}\right)\tau \\ e_T^p &= \left(\frac{\gamma_e^p}{\tau_e}\right)\frac{\sigma_T}{R^2} \\ \gamma_e^p &= \sqrt{(\gamma^p)^2 + R^2(e_T^p)^2} \end{aligned}\right\}. \tag{9}$$

Note that the functional dependence of γ_e^p on τ_e is assumed to be the same as that of γ^p on τ for pure shear, so that

$$\gamma_e^p = \left[\frac{1}{G_s(\tau_e)} - \frac{1}{G}\right]\tau_e \tag{10}$$

where the function $G_s(\tau_e)$ is the pure shear secant modulus. E_T and G are the transverse and shear composite elastic moduli.

Combining the elastic and plastic strain components from (9) leads to

$$\left.\begin{aligned} \gamma &= \frac{\tau}{G} + \gamma^p = \left(\frac{1}{G} + \frac{\gamma_e^p}{\tau_e}\right)\tau \\ e_T &= \frac{\sigma_T}{E_T} + e_T^p = \left[\frac{1}{E_T} + \frac{1}{R^2}\left(\frac{\gamma_e^p}{\tau_e}\right)\right]\sigma_T \end{aligned}\right\}. \tag{11}$$

Equation (11) dictates that the following condition must be satisfied in order for the kink band material to experience proportional *loading*:

$$\frac{E_T}{G} = R^2 = \left(\frac{\sigma_{Ty}}{\tau_y}\right)^2 \tag{12}$$

which, along with (11), gives

$$\left.\begin{aligned} \gamma &= \frac{\tau}{G_s(\tau_e)} \\ e_T &= \frac{\sigma_T}{R^2 G_s(\tau_e)} \end{aligned}\right\}. \tag{13}$$

We adopt the simplifying assumption of proportional loading by assuming that (12)

is satisfied; this is a reasonable approximation for many polymer matrix composites (BUDIANSKY and FLECK, 1993). A total effective strain is defined by

$$\gamma_e \equiv \frac{\tau_e}{G_s(\tau_e)} \tag{14}$$

so that

$$\gamma_e = \sqrt{\gamma^2 + R^2 e_T^2} = \gamma_e^p + \frac{\tau_e}{G}. \tag{15}$$

Thus, γ_e is the sum of an elastic part, τ_e/G, and a plastic part, γ_e^p, defined in (9).

The strategy is now to re-express the equilibrium equation (2) in terms of τ_e and γ_e. Substituting the approximate kinematic conditions, (3) into (15) leads to an expression for the effective strain as a function of ϕ,

$$\gamma_e = \alpha\phi \tag{16}$$

where

$$\alpha \equiv \sqrt{1 + R^2 \tan^2 \beta}. \tag{17}$$

The numerator on the right-hand side of the equilibrium equation (2) is simplified via (13)–(16) to give,

$$\tau + \sigma_T \tan \beta = \alpha\tau_e. \tag{18}$$

Define the pure shear yield strain as $\gamma_y \equiv \tau_y/G$. The equilibrium equation (2) can then be rewritten as

$$s^\infty = \frac{t}{\bar{\omega} + \eta} \tag{19}$$

where $s^\infty \equiv \sigma^\infty/G^*$, $t \equiv \tau_e/t_y$, $\eta \equiv \gamma_e/\gamma_y$ and $\bar{\omega} \equiv \bar{\phi}/\gamma_y^*$ are non-dimensional variables and

$$\left.\begin{aligned} G^* &\equiv \alpha^2 G \\ \gamma_y^* &\equiv \gamma_y/\alpha \end{aligned}\right\}. \tag{20}$$

Using an idea first suggested by BATDORF and KO (1987), and developed by BUDIANSKY and FLECK (1993), a Considère diagram can be constructed to represent (19). On a plot with η as the abscissa and t as the ordinate, the equilibrium state is represented by a line of slope s^∞ and x-intercept of $-\bar{\omega}$ (see Fig. 2). If, on the same plot, the constitutive equation for monotonic loading,

$$\eta = \frac{G}{\tilde{G}_s(t)} t, \tag{21}$$

is given, where $\tilde{G}_s(t) \equiv G_s(\tau_e)$, then the critical microbuckling load for monotonic loading, s_c^∞, is such that the equilibrium line is tangential to the constitutive curve, as shown in Fig. 2. From (19) and (21), this is expressed by the two simultaneous equations

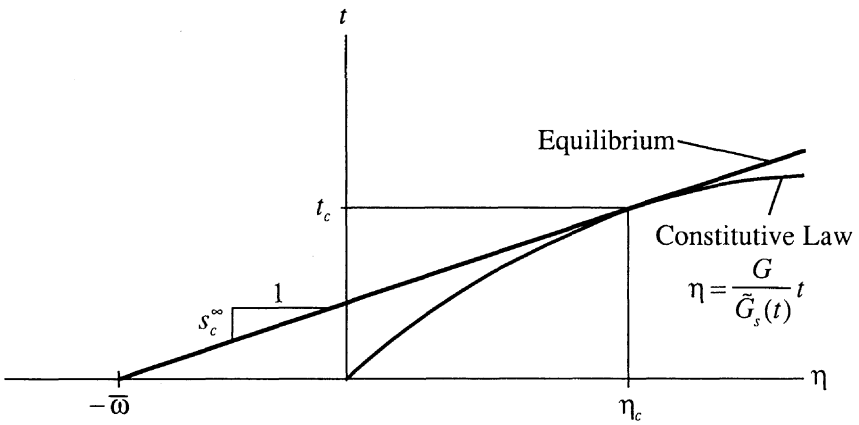

FIG. 2. Considère construction for calculation of the critical microbuckling stress s_c^∞ under monotonic loading.

$$\left.\begin{aligned} \frac{1}{s_c^\infty} &= \frac{\partial}{\partial t_c}\left[\frac{G}{\tilde{G}_s(t_c)} t_c\right] \\ \frac{G}{\tilde{G}_s(t_c)} t_c &= \frac{t_c}{s_c^\infty}\bar{\omega} \end{aligned}\right\} \tag{22}$$

for s_c^∞ and the effective strain at which microbuckling occurs, t_c. BUDIANSKY and FLECK (1993) have shown that for a Ramberg–Osgood composite material response, where the constitutive equation is

$$\frac{G}{\tilde{G}_s(t)} = 1 + \tfrac{3}{7} t^{n-1}, \tag{23}$$

with n a material parameter, (22) lead to the microbuckling solution

$$\left.\begin{aligned} t_c &= \left[\frac{7\bar{\omega}}{3(n-1)}\right]^{1/n} \\ s_c^\infty &= \frac{1}{1 + n\left(\frac{3}{7}\right)^{1/n}\left(\frac{\bar{\omega}}{n-1}\right)^{(n-1)/n}} \end{aligned}\right\}. \tag{24}$$

This form of Considère diagram will be utilized in the following analyses to illustrate the local kink band response to remote cyclic loading.

FATIGUE MICROBUCKLING

Mroz cyclic plasticity law; no ratchetting

In the analyses of compression–compression fatigue to follow, it is presumed that the remote axial load is initially increased monotonically from zero to s_{max}^∞, and then

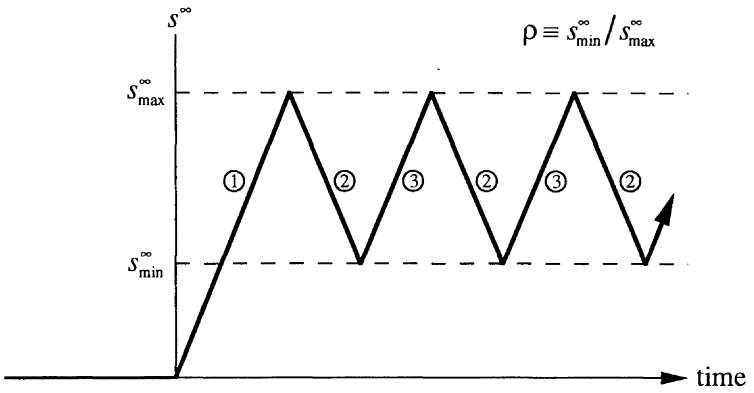

FIG. 3. Compression–compression fatigue loading history. Constant amplitude loading is assumed.

cycled steadily between s^∞_{max} and s^∞_{min} (see Fig. 3). The fatigue ratio ρ is defined as $\rho \equiv s^\infty_{min}/s^\infty_{max}$. During the initial loading, the composite constitutive behaviour is given by the composite monotonic response, as defined by (21). This equation and the equilibrium equation (19) can be used to determine the effective stress and strain within the kink band, t and η, as a function of s^∞ during this initial loading phase. The peak stress and strain, corresponding to s^∞_{max}, are defined as t_2 and η_2. The kink band stress–strain history is shown on a Considère diagram in Fig. 4. The segment of the history corresponding to the initial loading is labelled (1). It follows a path given by the constitutive equation (21) and terminates at the intersection with the line representing equilibrium when $s^\infty = s^\infty_{max}$, i.e. a line with slope s^∞_{max} and x-intercept $-\bar{\omega}$. This intersection occurs at the peak levels of stress and strain, t_2 and η_2. The corresponding segment of the remote axial load history in Fig. 3 is also labelled (1).

During unloading, when the remote axial load is reduced from s^∞_{max} to s^∞_{min}, the composite constitutive behaviour is given by the Mroz multiyield surface hardening rule (CHABOCHE, 1986). Since proportional loading is maintained, this response can be integrated up into the form of a deformation theory, giving

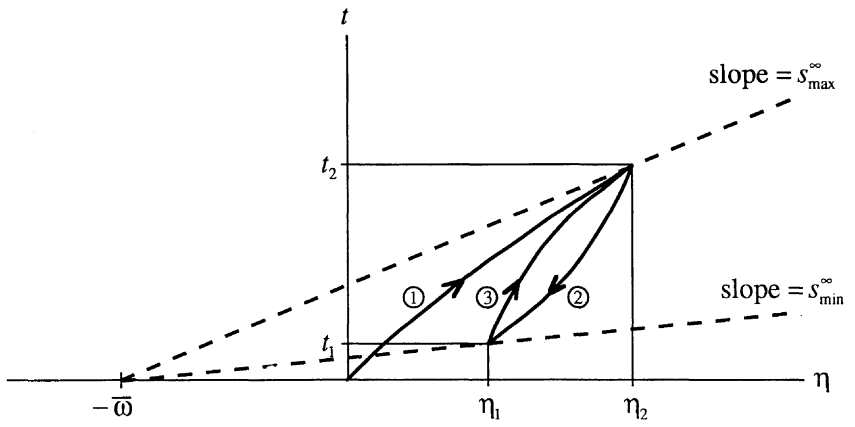

FIG. 4. Determination of the cyclic stress–strain history in a kink band using the Mroz plasticity law and a Considère construction.

$$\eta = \eta_2 - \frac{2G}{\tilde{G}_s\left(\frac{t_2 - t}{2}\right)}\left(\frac{t_2 - t}{2}\right). \tag{25}$$

Equation (25) is consistent with Masing's rule for fully reversed cyclic loading. The effective stress and strain in the kink band during this unloading phase of the cycle can be determined by combining (25) and the equilibrium equation (19). The minimum effective stress and strain, corresponding to the axial load $s^{\infty}_{\min}$, are defined as t_1 and η_1. On the Considère diagram (Fig. 4), this phase of the kink band stress–strain history is labelled (2). Similarly, the reloading phase of the stress–strain history, when the remote axial load is increased from $s^{\infty}_{\min}$ to $s^{\infty}_{\max}$, is characterized by the constitutive relation

$$\eta = \eta_1 + \frac{2G}{\tilde{G}_s\left(\frac{t - t_1}{2}\right)}\left(\frac{t - t_1}{2}\right) \tag{26}$$

and is labelled (3). The segments of the remote axial loading history shown in Fig. 3 are labelled as they correspond to segments of the stress–strain history of the Considère diagram in Fig. 4. Note that the constitutive equations (25) and (26) result in a closed cycle in the stress–strain space of the kink band, i.e. there is no ratchetting.

For the Coffin–Manson low-cycle fatigue law to be used, it is necessary to know the change in plastic strain per load cycle,

$$\Delta\eta^{\mathrm{p}} \equiv \eta^{\mathrm{p}}_2 - \eta^{\mathrm{p}}_1 = (\eta_2 - t_2) - (\eta_1 - t_1). \tag{27}$$

Using (25) and (26), (27) can be rewritten as

$$\Delta\eta^{\mathrm{p}} = \frac{2G}{\tilde{G}_s\left(\frac{\Delta t}{2}\right)}\left(\frac{\Delta t}{2}\right) - \Delta t \tag{28}$$

where $\Delta t \equiv t_2 - t_1$. The peak effective stress, t_2, is determined by combining the monotonic composite material response, (21), with the equilibrium condition, (19), where $s^{\infty} = s^{\infty}_{\max}$. Thus, t_2 is the solution of the equation

$$t_2 - s^{\infty}_{\max}\left[\frac{G}{\tilde{G}_s(t_2)}t_2 + \bar{\omega}\right] = 0. \tag{29}$$

The minimum effective stress, t_1, comes from combining (25) and (19) with $s^{\infty} = s^{\infty}_{\min}$. Thus, t_1 is the solution of the equation

$$t_1 - s^{\infty}_{\min}\left[\eta_2 - \frac{2G}{\tilde{G}_s[(t_2 - t_1)/2]}\left(\frac{t_2 - t_1}{2}\right) + \bar{\omega}\right] = 0. \tag{30}$$

Rewriting (30) in terms of Δt,

$$\Delta t - \left(1 - \frac{s^{\infty}_{\min}}{s^{\infty}_{\max}}\right) t_2 + \frac{2G}{\tilde{G}_s(\Delta t/2)} \left(\frac{\Delta t}{2}\right) s^{\infty}_{\min} = 0. \tag{31}$$

For a Ramberg–Osgood composite material response as given by (23), then (29), (31), and (28) become respectively,

$$t_2 - s^{\infty}_{\max}(t_2 + \tfrac{3}{7} t_2^n + \bar{\omega}) = 0, \tag{32}$$

$$\Delta t - \left(1 - \frac{s^{\infty}_{\min}}{s^{\infty}_{\max}}\right) t_2 + s^{\infty}_{\min}(\Delta t + \tfrac{6}{7}(\Delta t)^n + \bar{\omega}) = 0, \tag{33}$$

and

$$\Delta \eta^{\mathrm{p}} = \frac{6}{7} \left(\frac{\Delta t}{2}\right)^n. \tag{34}$$

To obtain $\Delta \eta^{\mathrm{p}}$ as a function of $s^{\infty}_{\max}$, $s^{\infty}_{\min}$, $\bar{\omega}$ and n, we solve (32) for t_2 and then (33) for Δt. Finally, we use (34) to calculate $\Delta \eta^{\mathrm{p}}$.

Note that the peak load in the fatigue cycle must be less than the critical load for monotonic microbuckling given in (24), $s^{\infty}_{\max} < s^{\infty}_{\mathrm{c}}$. If this condition is not satisfied, (32) will not have a real, positive solution. In general, (32) has n solutions, but the positive real solution of smallest magnitude is the only one of interest here. This solution is readily obtained using a standard root finding algorithm and a modicum of care. The same applies for solving (33).

Once the change in effective plastic strain experienced by the kink band during a cycle of fatigue, $\Delta \eta^{\mathrm{p}}$, has been calculated, a Coffin–Manson type low-cycle fatigue relationship is used to determine the number of cycles at failure;

$$\frac{\Delta \eta^{\mathrm{p}}}{2} = \frac{\gamma'_{\mathrm{f}}}{\gamma_y} (2N_{\mathrm{f}})^{\mathrm{c}} \tag{35}$$

where γ'_{f} and c are material parameters and N_{f} is the number of cycles at failure. The more usual Coffin–Manson relationship is for normal uniaxial straining and takes the form (HERTZBERG, 1976)

$$\frac{\Delta \varepsilon^{\mathrm{p}}}{2} = \varepsilon'_{\mathrm{f}} (2N_{\mathrm{f}})^{c} \tag{36}$$

where $\Delta \varepsilon^{\mathrm{p}}$ is the change in normal plastic strain experienced during a cycle of fatigue (not normalized by the yield strain). The material fatigue parameter $\varepsilon'_{\mathrm{f}}$ is associated with (but not generally equal to) the normal strain at failure under monotonic uniaxial loading ε_{f}. Examples of typical parameter values for metals are $\varepsilon'_{\mathrm{f}} = 0.95$ and $c = -0.64$ for SAE 1015 steel and $\varepsilon'_{\mathrm{f}} = 0.42$ and $c = -0.65$ for 2014-T6 aluminium (HERTZBERG, 1976). To make use of tabulated values for the fatigue material parameters in (36), they need to be related to those in (35). We assume that the exponent parameters c in each equation are equivalent and that $\gamma'_{\mathrm{f}}/\varepsilon'_{\mathrm{f}} = \gamma_{\mathrm{f}}/\varepsilon_{\mathrm{f}}$ where γ_{f} is the pure shear failure strain.

An approximate relation between γ_{f} and ε_{f} can be established by assuming a von Mises type failure surface in stress space that depends only on the second stress

invariant J_2. Then, $\sigma_f = \sqrt{3}\tau_f$ where σ_f and τ_f are the monotonic normal and shear failure stresses, and the failure strains ε_f and γ_f are related by the work statement $\sigma_f \varepsilon_f = \tau_f \gamma_f$. Hence,

$$\frac{\gamma_f'}{\varepsilon_f'} = \frac{\gamma_f}{\varepsilon_f} = \frac{\sigma_f}{\tau_f} = \sqrt{3}. \tag{37}$$

Predictions of the Mroz plasticity law

The predictions of the model for the parameter values $c = -0.65$, $\gamma_f'/\gamma_y = 360$ and $\bar{\omega} = 100$ are given in Fig. 5. These values are illustrative of those for long aligned fibre–metal matrix composites, as detailed below. Ramberg–Osgood parameter values of $n = 3$ and 5 and fatigue ratio values of $\rho = 0$, 0.25 and 0.5 are considered. The results are presented as the range of cyclic loading, $\Delta s^\infty \equiv s^\infty_{max} - s^\infty_{min}$, versus the number of cycles at failure, N_f. An upper limit on the values of Δs^∞ which are consistent with fatigue microbuckling (as opposed to monotonic microbuckling) is given by

$$\Delta s^\infty < (1-\rho) s_c^\infty \tag{38}$$

where s_c^∞ is the monotonic microbuckling load given by (24). The transition from fatigue to monotonic microbuckling, as Δs^∞ is increased, is represented in Fig. 5 and in subsequent figures by a cross; to the left of the cross runs a horizontal line $\Delta s^\infty = (1-\rho) s_c^\infty$. This transition does not generally occur at $N_f = 1$. The reason is that monotonic microbuckling and microbuckling by low cycle fatigue are different phenomena. Monotonic microbuckling involves plastic collapse while the results shown in Fig. 5 are based on the idea of localized fatigue failure (described by a Coffin–Manson low-cycle fatigue relationship) within the kink band. The model

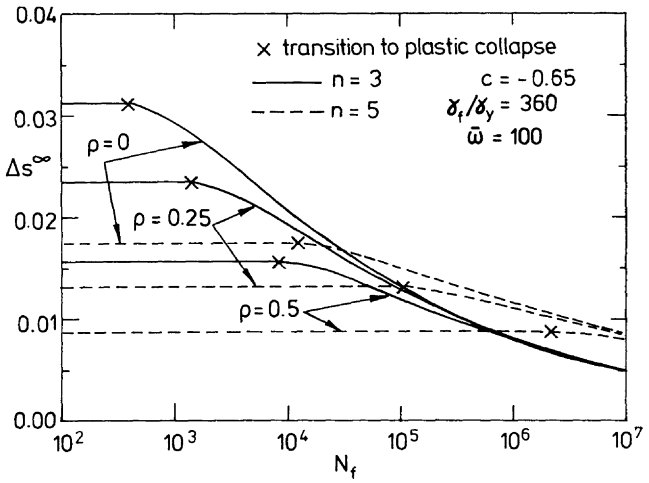

FIG. 5. Effect of load ratio ρ and strain hardening index n upon the low cycle fatigue response. The amplitude of remote cyclic loading Δs^∞ is plotted against the predicted fatigue life N_f using the Mroz plasticity law and a Coffin–Manson low cycle fatigue law. The horizontal lines to the left of the crosses represent the level of Δs^∞ above which monotonic microbuckling ($N_f = 1$) occurs by plastic collapse.

predicts that as Δs^{∞} increases there is a discontinuous jump in the number of cycles to failure N_f at the transition from fatigue to monotonic microbuckling.

Provided that the peak remote load s^{∞}_{max} is not near the monotonic microbuckling load, the number of cycles to failure is nearly independent of the fatigue ratio, ρ. There is a strong dependence on the Ramberg–Osgood parameter, n: the fatigue resistance increases strongly with increasing n. The dependence of the fatigue microbuckling predictions on the Coffin–Manson composite fatigue parameters is examined in Fig. 6. The range of cyclic loading versus the number of cycles at failure is given for $n = 3$, $\bar{\omega} = 100$ and $\rho = 0$ with fatigue parameter values of $c = -0.5$ and -0.8 and $\gamma'_f/\gamma_y = 100$, 200 and 400. These values for c and γ'_f/γ_y span the expected range for metal matrix composites. There is a strong dependence on the parameter c and a weaker dependence on γ'_f/γ_y. The number of cycles at failure N_f increases as γ'_f/γ_y increases and as c approaches zero.

Comparison with experimental data

Experimental results on compressive fatigue microbuckling of a 50 volume percent alumina (Al_2O_3) fibre, aluminium–lithium alloy (Al–2.5% Li) matrix composite have been presented by HUANG and WANG (1989). These results can be compared to the model predictions by choosing material properties and parameters which match, as nearly as can be determined, those of the actual composite. The data from Huang and Wang are presented as the number of cycles to failure N_f as a function of applied axial load σ^{∞}_{max} with $\rho = \sigma^{\infty}_{min} = 0$. In order to compare the data with the non-dimensional predictions of the model, a value for G^* is required. Assume first that $R = 2$ and $\beta = 20^{\circ}$ so that $\alpha = 1.24$. These values are typical for many unidirectional fibre composites. Young's moduli for the fibre and matrix, respectively, are $E_f = 380$ GPa and $E_m = 80$ GPa (HUANG and WANG, 1989). Assuming Poisson's ratio is $\nu = 0.3$ (and ignoring elastic anisotropy) for both the fibre and the matrix, the respective shear moduli are then $G_f = 150$ GPa and $G_m = 30$ GPa. The approximate rule of

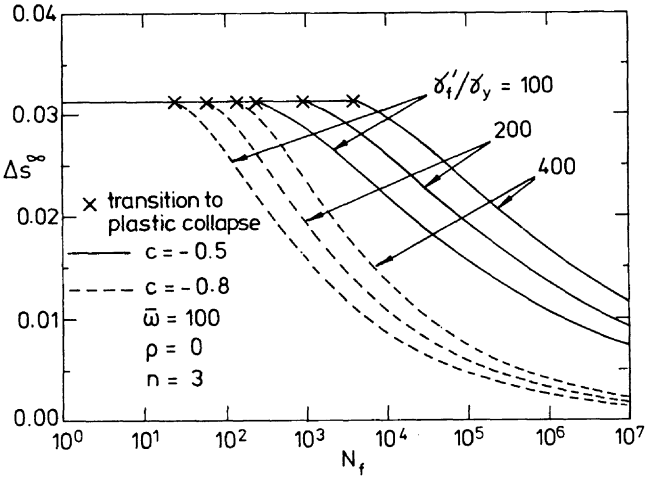

FIG. 6. An examination of the dependence of the model predictions on the Coffin–Manson fatigue law parameters. The horizontal lines to the left of the crosses represent the level of Δs^{∞} above which monotonic microbuckling ($N_f = 1$) due to plastic collapse occurs.

mixtures formula, $1/G \approx v_{f//}/G_f + (1-v_f)/G_m$ where $v_f = 0.5$ is the fibre volume fraction, is used to obtain the shear modulus for the composite examined by Huang and Wang: $G = 50$ GPa. The adjusted shear modulus, by (20), is then $G^* = 77$ GPa. For the fatigue law, (35), the index c is taken to be the same as that for aluminium, $c = -0.65$. A knock down factor of $(1-v_f)$ is imposed on the value of ε_f' for aluminium, to account for the presence of rigid fibres; thus $\varepsilon_f' = 0.42(1-v_f) = 0.21$ and, from (37), $\gamma_f'/\gamma_y = 360$ where the shear yield strain has been taken to be $\gamma_y = 0.001$.

A direct comparison is made with the experimental results of HUANG and WANG (1989) in Fig. 7. A range of initial fibre misalignment $\bar{\omega} = 50$–200, which corresponds to $\bar{\phi} = 2.3$–$9.2°$, is considered. The experimental results indicate a much more rapid increase in the fatigue life N_f as the amplitude of fatigue loading is decreased than is predicted by the model. There is also no evidence of a discontinuous jump in the number of cycles at failure as the failure mechanism goes from monotonic microbuckling to fatigue microbuckling. There is insufficient agreement between any of the model prediction curves and the experimental data to draw firm conclusions about appropriate values of $\bar{\omega}$ and n. Experience with polymer matrix composites suggests a value for $\bar{\phi}$ in the range 2–4° which with $\gamma_y = 0.001$ and $\alpha = 1.24$ corresponds to $\bar{\omega}$ in the range 43–86. This is consistent with the results shown in Fig. 7.

It is possible to choose the fatigue law parameter γ_f'/γ_y so that, when $s_{max}^{\infty} = s_c^{\infty}$, the number of cycles to failure is $N_f = 1$. Such a choice of γ_f'/γ_y bears no relationship to tabulated values of fatigue law parameters based on uniaxial fatigue tests, and will be different for each value of Ramberg–Osgood parameter n and fatigue ratio ρ. The value of γ_f'/γ_y is based on a comparison between the fatigue response and microbuckling by a plastic collapse mechanism; these phenomena appear to be distinct. Thus, choosing γ_f'/γ_y in this manner is essentially a curve fitting procedure. The results are shown in Fig. 8 with the value of γ_f'/γ_y indicated for each curve. The fatigue parameter $c = -0.65$, the initial fibre misalignment $\bar{\omega} = 100$, fatigue ratios of $\rho = 0$

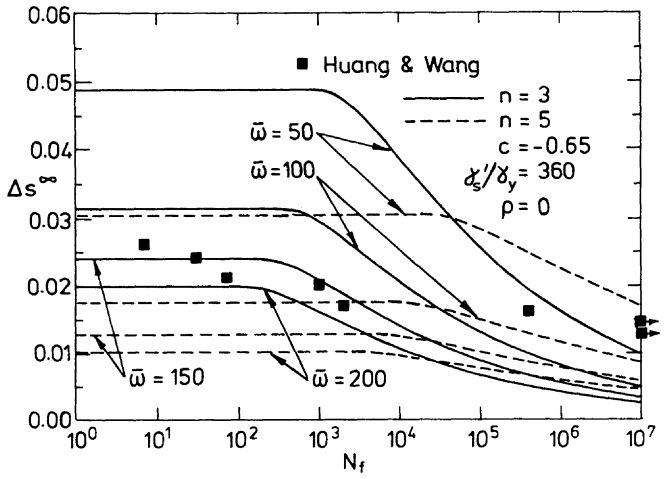

FIG. 7. Comparison of predicted fatigue lives by the Mroz plasticity law with measured fatigue lives of an alumina–aluminium alloy composite (HUANG and WANG, 1989). In presenting the experimental results it is assumed that $\alpha = 1.24$. For the theoretical curves the transition point between low cycle fatigue and plastic collapse is not shown explicitly. The horizontal lines represent the level of Δs^{∞} above which monotonic microbuckling ($N_f = 1$) due to plastic collapse occurs.

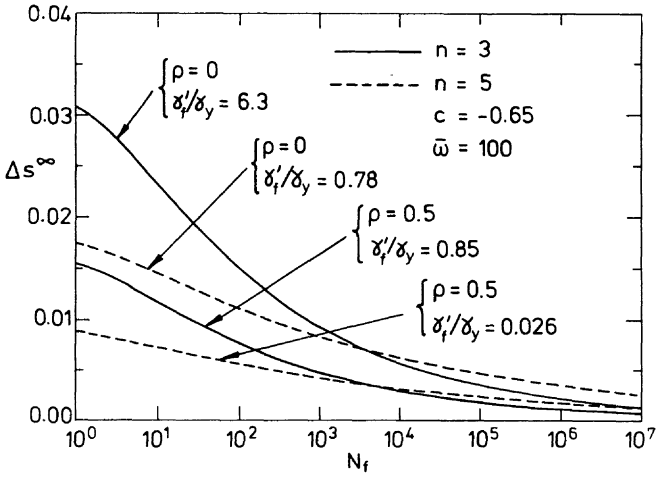

FIG. 8. Predicted fatigue life using the Mroz plasticity law and a Coffin-Manson low cycle fatigue law. The parameters of the model have been adjusted so that failure occurs in fatigue at a life $N_f = 1$ at the same load as the plastic instability load.

and 0.5, and Ramberg–Osgood parameter values of $n = 3$ and 5 are considered. The fatigue curves in Fig. 8 indicate a more rapid increase in N_f with decreasing Δs^∞ than was previously the case, but with a greater dependence on the fatigue ratio ρ. The model predictions, for different values of initial fibre misalignment $\bar{\omega}$ and Ramberg–Osgood parameter n, are compared with the experimental results (HUANG and WANG, 1989) in Fig. 9. The predictions for Ramberg–Osgood parameter $n = 5$ and initial fibre misalignment $\bar{\omega} = 50$ ($\gamma'_f/\gamma_y = 0.39$) provide the closest agreement with the data of Huang and Wang among those combinations of parameters that were considered. The correspondence is generally better than for the unmodified version of the model but still predicts a steeper fatigue life curve than observed experimentally.

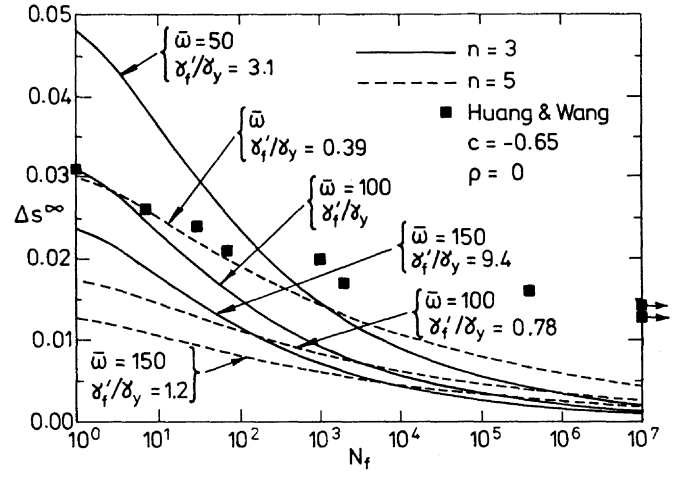

FIG. 9. Comparison of predicted fatigue lives with measured fatigue lives of an alumina–aluminium alloy composites (HUANG and WANG, 1989). The parameters of the model have been adjusted so that failure occurs in fatigue at a life $N_f = 1$ at the same load as the plastic instability load. In presenting the experimental results it is assumed that $\alpha = 1.24$.

Armstrong and Frederick cyclic plasticity law; ratchetting

As an alternative to the Mroz cyclic plasticity law, a non-linear kinematic hardening rule (ARMSTRONG and FREDERICK, 1966; CHABOCHE, 1986) is used to incorporate ratchetting within the kink band. For this proportional loading application, kinematic hardening means that the yield condition can be expressed as

$$|t-X| = 1 \tag{39}$$

where X is defined as the centre of the yield surface. The strain hardening rule proposed by ARMSTRONG and FREDERICK (1966) can be expressed as

$$\frac{\mathrm{d}X}{\mathrm{d}\eta^{\mathrm{p}}} = \frac{\mathrm{d}t}{\mathrm{d}\eta^{\mathrm{p}}} = \tfrac{2}{3}\lambda - \mu X \tag{40}$$

for a positive increment of plastic strain and

$$\frac{\mathrm{d}X}{\mathrm{d}\eta^{\mathrm{p}}} = \frac{\mathrm{d}t}{\mathrm{d}\eta^{\mathrm{p}}} = \tfrac{2}{3}\lambda + \mu X \tag{41}$$

for a negative increment of plastic strain. The strain hardening parameters λ and μ are material constants. If a material element described by (40) and (41) experiences cyclic loading with a non-zero mean stress, and $\mu \neq 0$, then ratchetting occurs. If $\mu = 0$, then ratchetting does not occur and the material has a linear strain hardening response. Equations (40) and (41) can be integrated to give the following solution for plastic straining

$$\eta = t+\eta^{\mathrm{p}} = t+\eta_0^{\mathrm{p}} - \frac{1}{\mu}\ln\left[\frac{1-\dfrac{3\mu}{2\lambda}X}{1-\dfrac{3\mu}{2\lambda}X_0}\right] \quad \text{when} \quad t = X+1 \tag{42a}$$

$$\eta = t+\eta^{\mathrm{p}} = t+\eta_0^{\mathrm{p}} + \frac{1}{\mu}\ln\left[\frac{1+\dfrac{3\mu}{2\lambda}X}{1+\dfrac{3\mu}{2\lambda}X_0}\right] \quad \text{when} \quad t = X-1 \tag{42b}$$

where X_0 and η_0^{p} represent a point in the plastic stress–strain history not separated from the current point by a reversal in plastic straining. For example, for positive plastic straining when $t = X+1$, X_0 and η_0^{p} in (42a) represent some point in the current interval of positive plastic straining. Note that, regardless of the value of X_0 and η_0^{p}, the requirement for finite η,

$$|X| < \frac{2\lambda}{3\mu}, \tag{43}$$

always holds.

As in the previous analysis of the Mroz cyclic plasticity law, the remote uniaxial loading history is as shown in Fig. 3. During initial loading, when s^{∞} is increased

monotonically from zero to s^{∞}_{max}, the material response is initially elastic, $\eta = t$, until $t = 1$. Then the response is given by (42a) with $X_0 = \eta^p_0 = 0$. Referring to the equilibrium equation (19), if $s^{\infty}_{max} < (1+\bar{\omega})^{-1}$ then the material in the kink band will not reach the yield condition. At the other extreme, s^{∞} must be less than s^{∞}_{cl}, the critical load for monotonic microbuckling. s^{∞}_{cl} can be calculated by equating (42a) and the equilibrium equation (19),

$$\frac{t_{cl}}{s^{\infty}_{cl}} - \bar{\omega} = t_{cl} - \frac{1}{\mu}\ln\left[1 - \frac{3\mu}{2\lambda}(t_{cl}-1)\right], \tag{44}$$

and their derivative with respect to t [see (22)],

$$\frac{1}{s^{\infty}_{cl}} = 1 + \left[\frac{2\lambda}{3} - \mu(t_{cl}-1)\right]^{-1}, \tag{45}$$

where t_{cl} is the critical effective stress within the kink band corresponding to s^{∞}_{cl}. Combining (44) and (45), t_{cl} is given by the solution to

$$\frac{t_{cl}}{\dfrac{2\lambda}{3} - \mu(t_{cl}-1)} + \frac{1}{\mu}\ln\left[1 - \frac{3\mu}{2\lambda}(t_{cl}-1)\right] - \bar{\omega} = 0 \tag{46}$$

and s^{∞}_{cl} is then given by (45). If $(1+\bar{\omega})^{-1} < s^{\infty}_{max} < s^{\infty}_{cl}$, then t_1 and η_1 are defined as the effective stress and strain within the kink band at the peak remote load s^{∞}_{max} during the initial loading. This point in kink band stress–strain space is labelled (η_1, t_1) in the Considère diagram shown in Fig. 10. Equating the equilibrium equation (19) and the constitutive equation (42a), t_1 is given by the solution to

$$\left(1 - \frac{1}{s^{\infty}_{max}}\right)t_1 - \frac{1}{\mu}\ln\left[1 - \frac{3\mu}{2\lambda}(t_1-1)\right] + \bar{\omega} = 0 \tag{47}$$

and η_1 is given by the equilibrium equation (19).

During the subsequent unloading phase of the fatigue cycle, when the remote

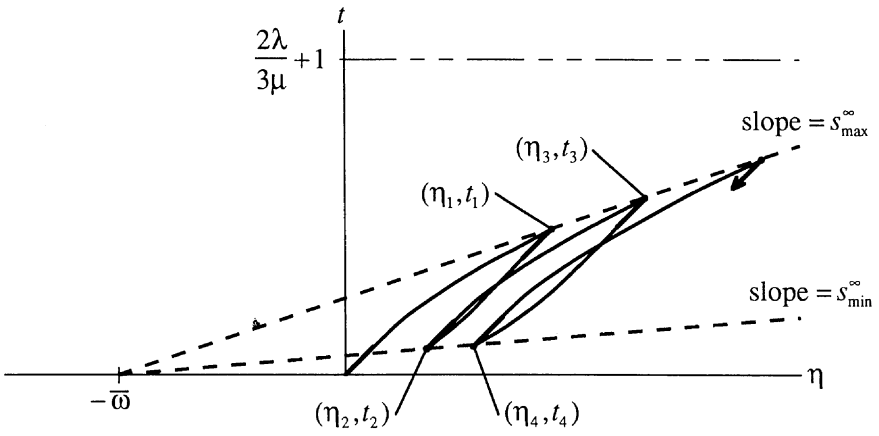

FIG. 10. Determination of the cyclic stress–strain history in a kink band using the Frederick–Armstrong ratchetting law and a Considère construction.

uniaxial load is reduced from $s^{\infty}_{\max}$ to $s^{\infty}_{\min}$, the kink band response is initially elastic, $\eta = \eta_1 - t_1 + t$, until $t = t_1 - 2$. Thus, if

$$s^{\infty}_{\min} > \frac{t_1 - 2}{\eta_1 - 2 + \bar{\omega}}, \tag{48}$$

then the first unloading, and all subsequent fatigue cycling, will involve only elastic deformation of the kink band and no ratchetting will occur. Otherwise, ratchetting will occur and plastic strain will accumulate until the kink band suffers a plastic collapse. In the analysis to follow, consecutive points in kink band stress–strain space, corresponding to values in the remote loading history of $s^{\infty}_{\max}$ and $s^{\infty}_{\min}$, are numbered sequentially (see Fig. 10). During fatigue cycle j, the values of stress and strain in the kink band when $s^{\infty} = s^{\infty}_{\max}$ are t_{2j-1} and η_{2j-1} and the values when $s^{\infty} = s^{\infty}_{\min}$ are t_{2j} and η_{2j}.

During the loading phase of a fatigue cycle j, the kink band constitutive response is given by (42a) with $X_0 = t_{2(j-1)} + 1$ and $\eta^{\mathrm{p}}_0 = \eta_{2(j-1)} - t_{2(j-1)}$. The values of $t_{2(j-1)}$ and $\eta_{2(j-1)}$ correspond to stress and strain in the kink band when $s^{\infty} = s^{\infty}_{\min}$ during the previous fatigue cycle and are assumed to be known. The critical load for plastic collapse of the kink band during this loading phase, s^{∞}_{cj}, and the corresponding effective stress, t_{cj}, are given by the solution to the equations

$$\frac{t_{cj}}{\dfrac{2\lambda}{3} - \mu(t_{cj} - 1)} - \eta_{2(j-1)} + t_{2(j-1)} + \frac{1}{\mu} \ln \left[\frac{1 - \dfrac{3\mu}{2\lambda}(t_{cj} - 1)}{1 - \dfrac{3\mu}{2\lambda}(t_{2(j-1)} + 1)} \right] - \bar{\omega} = 0 \tag{49}$$

$$s^{\infty}_{cj} = 1 - \frac{1}{\dfrac{2\lambda}{3} - \mu(t_{cj} - 1) + 1}. \tag{50}$$

If $s^{\infty}_{cj} < s^{\infty}_{\max}$ then the kink band experiences plastic collapse during this fatigue cycle. If not, the peak effective stress during this cycle, t_{2j-1}, is given by the solution to the equation

$$\left(1 - \frac{1}{s^{\infty}_{\max}}\right) t_{2j-1} + \eta_{2(j-1)} - t_{2(j-1)} - \frac{1}{\mu} \ln \left[\frac{1 - \dfrac{3\mu}{2\lambda}(t_{2j-1} - 1)}{1 - \dfrac{3\mu}{2\lambda}(t_{2(j-1)} + 1)} \right] + \bar{\omega} = 0 \tag{51}$$

and the corresponding effective strain, η_{2j-1}, is given by the equilibrium equation (19). Note that (46), (45) and (47) can be recovered from (49), (50) and (51), respectively, by letting $j = 1$ and $t_0 = \eta_0 = -1$.

During the unloading phase of a fatigue cycle j, the kink band constitutive response is given by (42b) with $X_0 = t_{2j-1} - 1$ and $\eta^{\mathrm{p}}_0 = \eta_{2j-1} - t_{2j-1}$. The values of t_{2j-1} and η_{2j-1} are known from the previous analysis of the loading phase of fatigue cycle j. The minimum effective stress at the end of this fatigue cycle, t_{2j}, when $s^{\infty} = s^{\infty}_{\min}$, is given by the solution to the equation

$$\left(1-\frac{1}{s^{\infty}_{\min}}\right)t_{2j}+\eta_{2j-1}-t_{2j-1}+\frac{1}{\mu}\ln\left[\frac{1+\dfrac{3\mu}{2\lambda}(t_{2j}+1)}{1+\dfrac{3\mu}{2\lambda}(t_{2j-1}-1)}\right]+\bar{\omega}=0 \qquad (52)$$

and the corresponding effective strain, η_{2j}, is given by the equilibrium equation (19).

To determine the number of fatigue cycles to failure, N_f, for given values of $s^{\infty}_{\max}$, $s^{\infty}_{\min}$, λ, μ and $\bar{\omega}$, first determine that $s^{\infty}_{\max} < s^{\infty}_{cl}$ as determined by (45) and (46); otherwise, the kink band will experience plastic collapse before fatigue cycling can commence, i.e. $N_f = 1$. Use (47) to determine t_1 and η_1. If the condition given by (48) is satisfied, then $N_f \to \infty$, so long as fatigue failure is assumed to be caused by the plastic collapse mechanism (as opposed to a Coffin–Manson fatigue law of the type used in the non-ratchetting analysis). Use (51) and (52) to proceed sequentially through fatigue cycles, calculating extreme values of effective stress and strain in the kink band. For the loading phase of each fatigue cycle j, use (49) and (50) to determine whether the kink band suffers plastic collapse. If so, then this is the cycle at which failure occurs and $N_f = j$. It is an interesting feature of this model that as plastic strain accumulates, the rate of ratchetting increases. Referring to Fig. 10, it can be seen that as η becomes larger, both the mean level of local stress and its amplitude increase resulting in larger increments of accumulated strain with each cycle of fatigue.

Predictions of the Armstrong and Frederick ratchetting law

The results for this plastic ratchetting model of fatigue microbuckling are shown in Figs 11 and 12. The range of remote loading is plotted against the number of fatigue cycles to failure. In Fig. 11 an initial fibre misalignment $\bar{\omega} = 100$, the fatigue ratio values of $\rho = 0$, 0.25 and 0.5 and strain hardening parameter values of $\lambda = 0.5$ and 1.0 and $\mu = 0.05$ are considered. In Fig. 12 strain hardening parameter values of $\mu = 0.04$, 0.05 and 0.06 are considered while $\rho = 0$ is kept fixed. The strain hardening

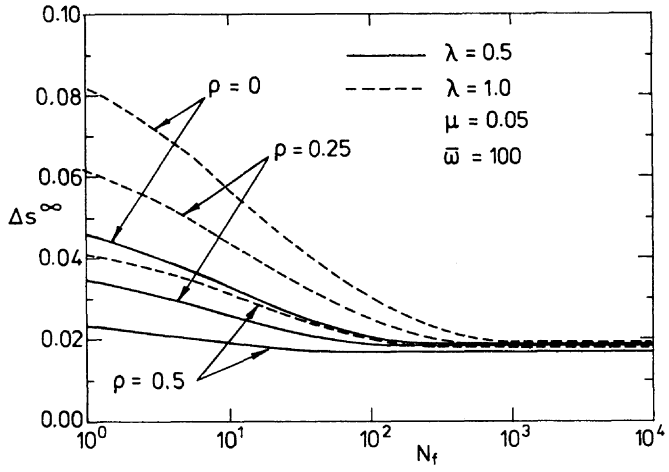

FIG. 11. The amplitude of remote cyclic loading Δs^{∞} versus the predicted fatigue life N_f based on the Frederick–Armstrong ratchetting law and failure by a plastic collapse mechanism. The effect of load ratio ρ and hardening parameter λ on fatigue response is explored.

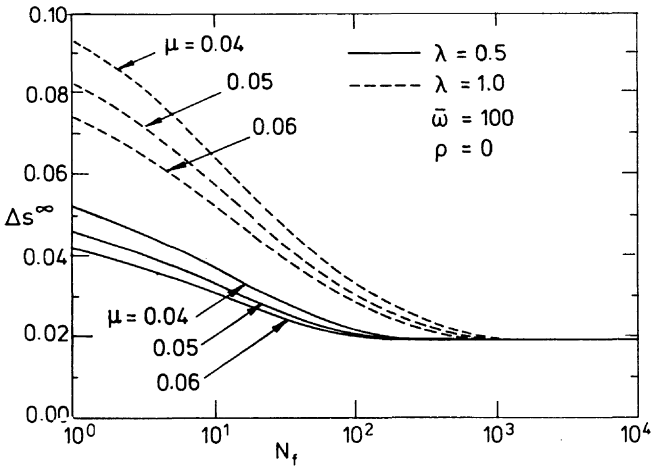

FIG. 12. The amplitude of remote cyclic loading Δs^∞ versus the predicted fatigue life N_f based on the Frederick–Armstrong ratchetting law and failure by a plastic collapse mechanism. The effect of the Frederick–Armstrong cyclic plasticity parameters λ and μ on fatigue response is explored.

parameters used were chosen to represent a range of likely values for an aluminium alloy matrix composite as inferred from experimental studies on copper ($\mu = 0.30$, $\lambda = 0.55$) and rail steel ($\mu = 0.0083$, $\lambda = 0.42$) reported by BOWER (1989). Directly measured values for either the aluminium–lithium matrix composite or its constituents are not available. The resulting fatigue life curves are approximately bi-linear on a logarithmic–linear scale. As the remote loading amplitude is reduced from the level of monotonic microbuckling, the logarithmic number of cycles to failure increases nearly linearly until the threshold level of infinite fatigue life is reached. At and below this threshold loading amplitude the composite experiences only elastic straining. This threshold loading amplitude is nearly independent of the strain hardening parameters and the fatigue ratio. At a given loading amplitude Δs^∞, the fatigue life N_f increases rapidly as the strain hardening parameter λ increases and as either the parameter μ or the fatigue ratio ρ decreases.

Comparison with experimental data

The experimental results of HUANG and WANG (1989) are given in Fig. 13 along with those of the ratchetting model. In the absence of directly measured values for aluminium alloy matrix composites, the strain hardening parameters $\mu = 0.05$ and 0.07 and $\lambda = 0.5$ and the initial fibre misalignments $\bar{\omega} = 100$, 150 and 200 where chosen partly on the basis of inferences drawn from the strain hardening parameters of other materials and partly in order to match the experimental results. The best match, for these strain hardening parameters, is obtained when $\bar{\omega} = 150$ corresponding to $\bar{\phi} = 7°$. In particular, the monotonic microbuckling load and the fatigue threshold are well matched. HUANG and WANG (1989) interpreted their experimental results as bi-linear in nature (on a log–linear scale), which is in agreement with the model predictions, though the experimental results for the number of cycles at failure increase more rapidly as the remote loading amplitude is decreased. The ratchetting model predictions agree reasonably well with the data of Huang and Wang.

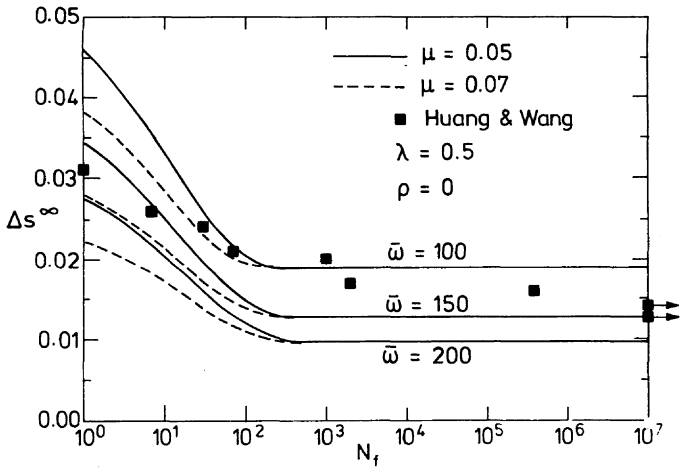

FIG. 13. Comparison of predicted fatigue lives, based on the Frederick–Armstrong ratchetting law and failure by a plastic collapse mechanism, with measured fatigue lives of an alumina–aluminium alloy composites (HUANG and WANG, 1989). In presenting the experimental results it is assumed that $\alpha = 1.24$.

CONCLUDING DISCUSSION

Two models have been presented for compressive fatigue microbuckling; the models are differentiated by the particular forms of cyclic plastic law used. Which of these is the more appropriate to some extent depends upon the composite under consideration. For the Al–2.5% Li matrix composite a comparison between experimental data (HUANG and WANG, 1989) and the model predictions, Figs 9 and 13, suggests that the cyclic plasticity law which includes ratchetting behaviour is the more appropriate. However, for polymer matrix composites, woods or other metal matrix composites this need not necessarily be the case. Unfortunately, there is a paucity of explicit experimental studies on compressive fatigue failure in fibre composites. The theoretical analysis presented here suggests that it is an important mode of failure. Short fatigue lives N_f are predicted at remote loading amplitudes Δs^∞ significantly below that required for monotonic microbuckling. This is borne out by the experimental results of HUANG and WANG (1989) who measured a fatigue life of only $N_f \approx 1000$ at a loading amplitude 65% of the monotonic microbuckling load. It remains to be established under which circumstances microbuckling is the dominant compressive fatigue failure mechanism. Huang and Wang reported microbuckling to be the dominant mechanism in their tests, but there are doubtless other competing mechanisms which may be important.

ACKNOWLEDGEMENT

Support from ONR grant 0014-91-J-1916 is gratefully acknowledged.

REFERENCES

ARGON, A. S. (1972) Fracture of composites. *Treatise of Materials Science and Technology*, Vol. 1. Academic Press, New York.

ARMSTRONG, P. J. and FREDERICK, C. O. (1966) A mathematical representation of the multiaxial bauschinger effect. C.E.G.B. Report RD/B/N 731.

BATDORF, S. B. and KO, R. W. C. (1987) Stress–strain behaviour and failure of unidirectional composites in combined compression and shear, Parts I and II. Internal report, School of Engineering and Applied Science, University of California, Los Angeles, CA, 90024.

BOWER, A. F. (1989) Cyclic hardening properties of hard-drawn copper and rail steel. *J. Mech. Phys. Solids* **37,** 455–470.

BUDIANSKY, B. and FLECK, N. A. (1993) Compressive failure of fibre composites. *J. Mech. Phys. Solids* **41,** 183–211.

CHABOCHE, J. L. (1986) Time-independent constitutive theories for cyclic plasticity. *Int. J. Plasticity* **1,** 149–188.

FLECK, N. A., DENG, L. and BUDIANSKY, B. (1993) Predictions of kink width in fibre composites. Submitted to *J. Appl. Mech.*

HERTZBERG, R. W. (1976) *Deformation and Fracture Mechanics of Engineering Materials.* John Wiley and Sons, New York.

HUANG, Y. H. and WANG, S. S. (1989). Compressive fatigue damage and associated property degradation of aluminum-matrix composite. *Proc. 4th Japan–U.S. Conf. on Composite Materials*, 27–29 June 1988, Washington, DC, pp. 606–632. Technomic, Westport, CT.

MROZ, Z. (1967) On the description of anisotropic work-hardening. *J. Mech. Phys. Solids* **15,** 163–175.

ROSEN, B. W. (1965) Mechanics of composite strengthening. *Fiber Composite Materials*, Am. Soc. Metals Seminar, Metals Park, Ohio, pp. 37–75.